small NANO MICRO

Gold nanoparticles

Facile Plasma-Enhanced Deposition of Ultrathin Crosslinked Amino Acid Films for Conformal Biometallization

*Kyle D. Anderson, Joseph M. Slocik, Michael E. McConney, Jesse O. Enlow, Rachel Jakubiak, Timothy J. Bunning, Rajesh R. Naik, and Vladimir V. Tsukruk**

***A** novel method for the facile fabrication of conformal, ultrathin, and uniform synthetic amino acid coatings on a variety of practical surfaces by plasma-enhanced chemical vapor deposition is introduced. Tyrosine, which is utilized as an agent to reduce gold nanoparticles from solution, is sublimed into the plasma field and directly deposited on a variety of substrates to form a homogeneous, conformal, and robust polyamino acid coating in a one-step, solvent-free process. This approach is applicable to many practical surfaces and allows surface-induced biometallization while avoiding multiple wet-chemistry treatments that can damage many soft materials. Moreover, by placing a mask over the substrate during deposition, the tyrosine coating can be micropatterned. Upon its exposure to a solution of gold chloride, a network of gold nanoparticles forms on the surface, replicating the initial micropattern. This method of templated biometallization is adaptable to a variety of practical inorganic and organic substrates, such as silicon, glass, nitrocellulose, polystyrene, polydimethylsiloxane, polytetrafluoroethylene, polyethylene, and woven silk fibers. No special pretreatment is necessary, and the technique results in a rapid, conformal amino acid coating that can be utilized for further biometallization.*

Keywords:
- biometallization
- gold nanoparticles
- plasma-enhanced chemical vapor deposition
- tyrosine

1. Introduction

Bioenabled methods are used to form inorganic coatings and nanoparticles composed of, for example, gold, silver, platinum, titania, silicates, calcinates, and iron, through the reduction of the corresponding ions with biomolecules (DNA, amino acids, proteins, and peptides), which act as nucleation sites, templates, and reducing agents.[1–10] A wide range of applications makes the method extremely useful for directed assembly, in which a targeted surface can be coated with the biomolecules and exposed to a solution containing the desired ions to be deposited. Reduction to form nano- and microparticles or even uniform coatings will only occur at activated sites on the deposited biorelevant layer.[11–14] This coating method allows a directed placement of inorganic nanoparticles on a surface through direct nanoparticle formation on materials that may be otherwise difficult to coat. Additionally, nanoparticles can be directed to form at specific locations on the surface by pattering the biomolecular layer during plasma deposition or by microprinting.[15] This method of nanoparticle formation allows for more functional and diverse uses of hybrid nanomaterials in applications such as optical sensing and responsive materials.[16]

[*] Prof. V. V. Tsukruk, K. D. Anderson, M. E. McConney
School of Materials Science and Engineering and
School of Polymer, Textile, and Fiber Engineering
Georgia Institute of Technology,
Atlanta, GA 30332-0245 (USA)
E-mail: vladimir@mse.gatech.edu
Dr. J. M. Slocik, J. O. Enlow, Dr. R. Jakubiak, Dr. T. J. Bunning, Dr. R. R. Naik
Materials and Manufacturing Directorate
Air Force Research Laboratory
Wright-Patterson Air Force Base
Dayton, OH 45433-7702 (USA)

DOI: 10.1002/smll.200801843

It is well known that amino acids such as lysine, tyrosine, and dopamine are effective agents for the reduction of noble metal nanoparticles from solution, due to the amine and hydroxy groups in the molecules that effectively reduce gold.[17–19] By coating a substrate surface with polytyrosine, gold nanoparticles can be reduced directly from solution to a desired surface coverage density.[20] Traditional techniques for fabricating these types of nanoscale coatings include methods such as simple solution- and dipcasting, spin-casting, spin-assisted layer-by-layer (LbL) assembly, self-assembled monolayer formation, and Langmuir–Blodgett film formation.[21,22] To achieve uniform coverage of inorganic nanoparticles on the surface, the substrate to be coated would have to be immersed in an aqueous amino acid solution for prolonged times or chemically modified with an additional LbL coating on an existing Langmuir monolayer.[18,23–28] Such polyelectrolyte-assisted deposition of silaffin proteins was demonstrated to be an effective method for surface growth of monodisperse titania nanoparticles.[29,30] Several inherent drawbacks of this approach stem from the extensive exposure of the substrate to salt solution which can potentially leading to swelling, partial dissolution, corrosion, or additive leaching. In addition, prolonged exposure to aqueous solutions may lead to particle aggregation, non-uniform coverage, and surface defects. By developing a rapid, one-step, solvent-free, conformal method for depositing, templating, or mineralizing inorganic materials on surfaces, substrates not amenable to the traditional wet chemistry approaches may be utilized for mineralization.

Polymerization of amino acids, including tyrosine, as well as the formation of synthetic polyamino acids have been readily demonstrated through wet chemical means.[31,32] The method of in situ polymerization of tyrosine coatings proposed herein focuses on the utilization of plasma-enhanced chemical vapor deposition (PECVD) as a potential method to polymerize the tyrosine monomer in the plasma stream and directly deposit the polytyrosine on the substrate. This type of plasma polymerization reaction has been demonstrated previously with various organic molecules and amino acids to form thin films that can also be easily patterned through the use of a mask secured on the substrate.[33–39]

A major advantage of PECVD is that it allows dry tyrosine powder to be sublimed into the plasma stream and coated onto a variety of substrates, making the technique a quick alternative method to depositing tyrosine coatings through a wet chemistry approach. Another key advantage of PECVD is the dense and highly crosslinked conformal coatings over sharp corners, developed texture, heterogeneous and rough surfaces, as opposed to direct film transfer or casting from solution which can result in delamination and defects in film coverage on such non-ideal surfaces. Biometallization with PECVD-assisted deposition of bioenabling coatings has potential applications in the modulation of the conductivity and catalytic properties of the surface through particle deposition. The addition of inorganic nanoparticles can be used for the mediation of optical properties, micropatterning, creation of selective surfaces, and thermal microsensors along with other sensor applications.[40,41]

In this study, we demonstrate the plasma polymerization of tyrosine and the formation of ultrathin conformal coatings on a variety of practical materials, making them capable of selectively binding and reducing gold nanoparticles onto various surfaces. This method of tyrosine-coating formation allows the utilization of readily available L-tyrosine monomer to form highly crosslinked, robust, conformal, and functionalized polytyrosine coatings in a simple, rapid, one-step process that can be applied to a variety of substrates. This type of coating method will allow virtually any object to be uniformly coated with a functional bioenabling layer, yielding an unlimited number of prospective applications in which nanoparticle reduction is needed and providing a universal fabrication method to achieve this.

2. Results and Discussion

2.1. Film Deposition

In general, PECVD coatings have the advantage of being uniform across the surface with a minimum of defects and non-uniformities: the tyrosine films described herein were no exception. Tyrosine films deposited onto clean silicon wafers showed a uniform surface morphology over a $10 \times 10\ \mu m^2$ area (Figure 1a). No dewetting of the films was seen after removal from the deposition chamber, indicating that the deposited tyrosine is stable on the substrate and not prone to delamination owing to internal stresses.[42,43] The PECVD tyrosine films were robust and were not easily removed from the silicon mechanically or in solution. The films performed well under a tape test as they did not show significant change when tape was applied to the film and removed. The PECVD tyrosine films were also observed to be very smooth as indicated by a surface roughness of 0.4 nm over a $1 \times 1\ \mu m^2$

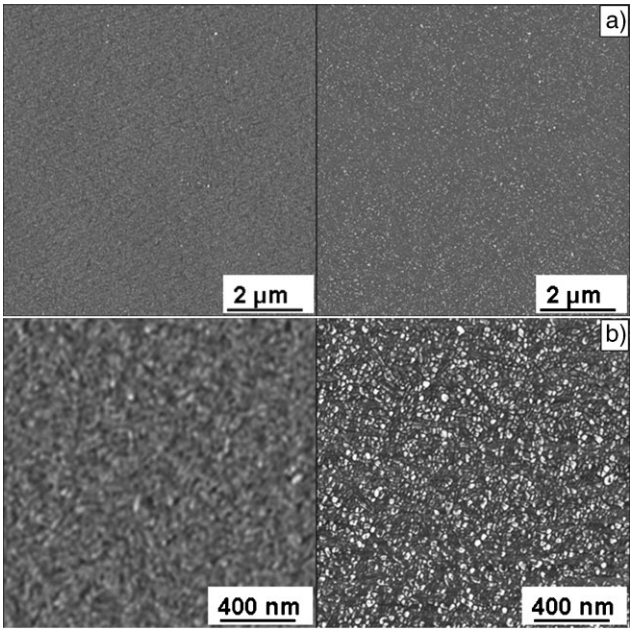

Figure 1. a) $10 \times 10\ \mu m^2$ and b) $2 \times 2\ \mu m^2$ AFM topography (left) and phase (right) of PECVD tyrosine film on silicon substrate prior to exposure to $HAuCl_4$. *Z* range of 10 nm for topography and 50° for phase in both images. Typical thickness and microroughness for the samples was 120 nm and 0.4 nm, respectively.

NANO MICRO small

surface area (Figure 1b). Under PECVD conditions, any part of the substrate facing perpendicular to the plasma stream was seen to be uniformly coated.

The tyrosine monomer was directly sublimed from the solid phase, with no modification, into the plasma stream, and is deposited on the substrate surface while undergoing considerable chain growth and crosslinking, both of which help to create stable, robust, and conformal ultrathin films on the surfaces. Monomers that are exposed to the high-energy plasma field under an inert atmosphere form reactive species, as previously described, allowing the radicals to react chemically with each other as they are polymerized and crosslinked into a network during deposition.[44–46] These films frequently exhibit unique physical properties that are controlled through the variation of the system parameters, such as chamber pressure, power, argon flow rate, and deposition time.[47–51]

Many samples were made under different deposition conditions to optimize thickness and uniformity of the films. The thickness of the film was controlled through variation of the deposition time (typically 8–12 min) at the optimized temperature, pressure, and argon flow rate listed. This gives a degree of control over the film formation, but it is still subject to the random nature of the plasma stream. We then kept the same deposition conditions for different deposition times and characterized thickness and microroughness. Typical film thicknesses were measured by ellipsometry to be between 100 and 150 nm, with the microroughness from $1 \times 1\ \mu m^2$ AFM images varying from 0.4 to 1 nm, depending on the particular sample.

The tyrosine coatings that were created were observed to be robust and resistant to mechanical wear and exposure to aqueous gold chloride solution. Preliminary observations of the films showed that they were stable under mild rubbing and not easily dissolved, even in solutions with high pH values. It is essential that the film be stable during the reduction of the gold and that it remains intact for the duration of the exposure to solutions. Film stability is critical to the subsequent biometallization process, so that the film will not delaminate from the substrate or dissolve in the solution when exposed to aqueous gold chloride. Delamination and film instability were seen in some films made under non-optimized chamber pressure conditions.

2.2. Composition of PECVD Films

During deposition of the tyrosine monomer it was critical to determine what, if any, changes occurred in the chemical structure of the molecule as a result of the heating and interaction with the plasma field followed by deposition onto a solid substrate. As the reduction of gold is dependant on key functional groups, such as the amine and hydroxy groups of the tyrosine molecule, these components must remain active on the surface of the film after plasma deposition for effective reduction of the gold nanoparticles.[52,53] If critical functional groups were cleaved or rendered nonfunctional, the ability of the film to reduce gold nanoparticles may be diminished or negated.

FTIR measurements on the solution-cast tyrosine film, plasma-deposited tyrosine film, and spin-cast polytyrosine film were conducted to elucidate the similarity of their chemical

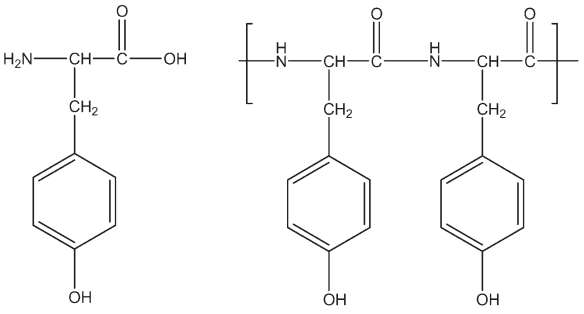

Figure 2. Chemical structures of L-tyrosine monomer and polytyrosine.

composition (Figure 2, Figure 3). The absorption peaks were assigned to key chemical groups of the plasma-polymerized tyrosine by using ACDLABS peak assignment software as well as comparison of known literature data.[44,54,55] For instance, NH_2 out-of-plane bending is seen at 829 cm^{-1}, in conjunction with a C–H stretch from the aromatic ring. The spectral shift from 876 cm^{-1} of this peak in L-tyrosine closer to 826 cm^{-1} seen in polytyrosine is a key marker that polymerization of the tyrosine monomer is, indeed, occurring in the plasma stream. This shift is most likely caused by amide bond formation, which occurs as the monomer polymerizes, and is similar to that observed in polytyrosine (Figure 2). This observed peak also leads us to infer that the amine group was retained in the plasma-polymerized tyrosine and is present on the surface coating — a strong indicator that gold reduction is possible on the plasma-deposited surface.

The presence of bands for aromatic rings in the FTIR spectrum is another strong indication that tyrosine remained, to a great extent, intact during deposition and did not undergo significant decomposition upon heating and exposure to the plasma. The peak seen in the PECVD tyrosine spectra at 1246 cm^{-1} corresponds to the bending OH vibration in the ring structure, and the peaks at 1332, 1515, and 1614 cm^{-1} arise

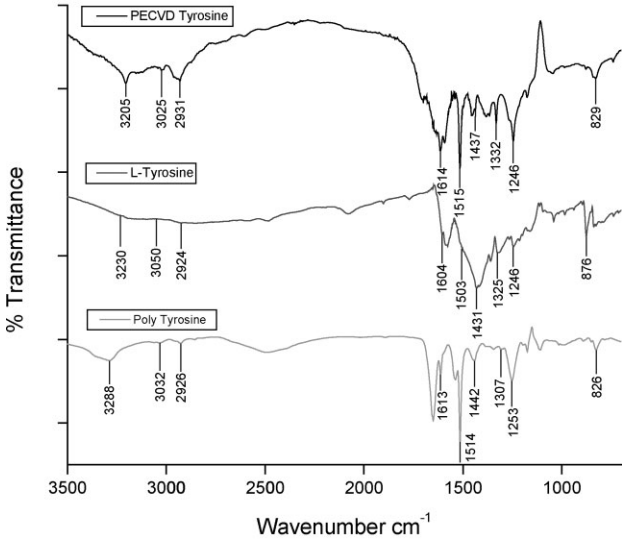

Figure 3. FTIR of films from PECVD tyrosine (top), L-tyrosine (center), and polytyrosine (bottom).

from the C–C double- and single-bond vibrations found in the aromatic ring. The peak for the alcohol group of the ring structure is seen at 3205 cm^{-1}, and a broad amine peak is seen at approximately 3000 cm^{-1}. These peaks remain for the most part consistent between the three different spectra, indicating no dramatic changes and main bond cleavage in the structure of the tyrosine monomer. The structural determinations of the different tyrosine samples by using FTIR were consistent with the chemical structure of polytyrosine known from the literature. The spectra indicate that there are no significant changes to the primary structure of the monomer from the plasma deposition. However, there is significant reaction of the L-tyrosine monomer, which then undergoes random crosslinking and network formation as the film is deposited on the substrate, while still maintaining the chemical functionality needed for reduction of the gold. Monomers become reactive after exposure to the plasma stream through the formation of ions and free radicals. The statistical majority of ions and free radicals are formed from the most reactive functional groups in the system. These ions and radical species can then react with others in many different, and often unpredictable, ways to form highly interwoven and linked structures. Owing to the random nature of the plasma, crosslinking becomes a statistical phenomenon, and a single reaction mechanism does not encompass the scope of the reactions that can occur at any ionized, available site on the polytyrosine chain.[44] This process leads to a network formation of the tyrosine which consists of many random crosslinks on the polytyrosine molecules and their fragments that do not always occur as predicted in theoretical models.

Optical characteristics of the PECVD tyrosine film were measured by spectroscopic ellipsometry and modeled with a Cauchy fit. The measured real refractive index n for a PECVD film of 120-nm thickness showed conventional behavior decreasing from 1.65 in the UV range to 1.60 at longer wavelength close to near-IR (Figure 4). At a wavelength of 543 nm the refractive index was relatively high, $n = 1.617$ (Figure 4). This value is much higher than traditional values for conventional synthetic polymers and corresponds to reported values of the refractive index for tyrosine crystals with a high packing coefficient.[54] This correspondence confirms dense local molecular packing of tyrosine residues within the PECVD coatings. Notably, the plasma-polymerized tyrosine film showed a higher refractive index than the spin-cast polytyrosine film with similar wavelength-dependent variation ($n = 1.441$ at $\lambda = 543$ nm) (Figure 4). This difference additionally confirmed that the PECVD tyrosine film was more densely packed and crosslinked than the spin-cast film of prepolymerized monomer. The greater density can be associated with high crosslinking and should allow effective reduction after exposure to the gold chloride solution.

The optical absorbance coefficient k, which represents the imaginary component of the complex refractive index, is also found to be very low for both spin-cast and PECVD tyrosine films, but much more so for the PECVD film (Figure 4). This indicates that at wavelengths greater than 400 nm, the films exhibits no optical absorption and are completely transparent. For example, at $\lambda = 542.7$ nm $k = 0.0022$ for the PECVD film and $k = 0.0031$ for the spin-cast polytyrosine film. Significant absorption is detected only in the UV region and can be associated with the presence of the phenyl ring with a UV-absorption band at around 250 nm.[56] At $\lambda = 250$ nm k is significant, reaching 0.122 for the PECVD film and 0.172 for the spin-cast polytyrosine film. Because of this low optical range absorbance in a wide window of visible wavelengths, these plasma-polymerized films can be used in applications that require optical transparency.

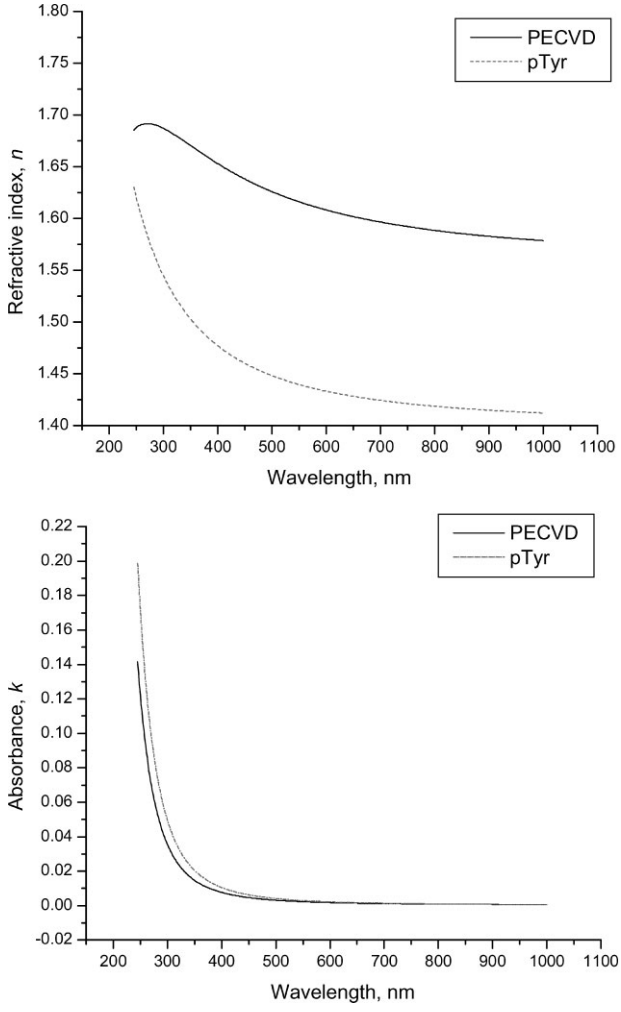

Figure 4. Refractive index n and absorbance coefficient k of PECVD tyrosine coating and spin-cast polytyrosine films from 245 to 1000 nm.

The results presented herein demonstrate that the formation of polymerized, highly crosslinked tyrosine networks readily occurs under the deposition conditions utilized. The plasma stream will impart enough energy to activate reactive sites (NH_2 and CO groups) on the L-tyrosine monomer and allow reactive species to form in the plasma which will polymerize and crosslink as they are deposited on the target substrate. The retention of the functionality of the PECVD film to reduce gold is the major point of interest in the chemical structure of plasma-deposited tyrosine and is the essential characteristic of the molecule to be retained during deposition, along with the ability to easily coat tyrosine onto various types of surfaces.

2.3. Biometallization on PECVD Tyrosine

Gold nanoparticles were reduced on the plasma-deposited tyrosine film by placing a solution of gold chloride ($HAuCl_4$) diluted in borate buffer on the film and allowing absorption to occur over a time period of 1–5 days. Gold nanoparticles that formed were typically within a 1–5-nm diameter range and were uniformly distributed on the surface at a high density (Figure 5a and b). AFM section analysis of the nanoparticles was used to determine the average nanoparticle diameter. This method was applied to the entire area to determine the number and average size of nanoparticles on the surface. The particle size distribution obtained from cross-sections was relatively narrow, yielding an average diameter of 2.2 ± 1 nm (Figure 5c, d). Larger gold clusters were observed to have formed on the surface occasionally, with sizes up to 20 nm (Figure 5b). EDX spot analysis of the particles reduced on the surface confirms their composition (Figure 6).

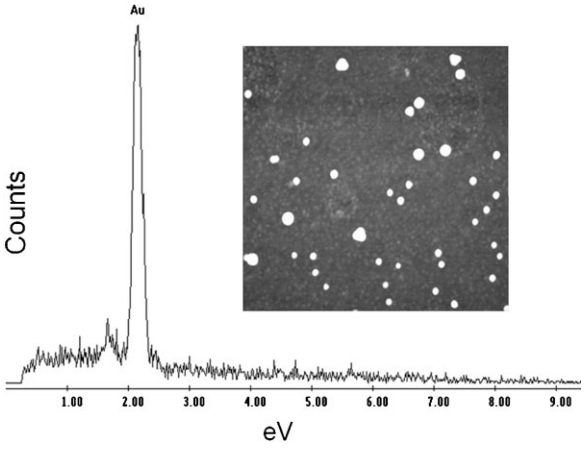

Figure 6. EDX analysis of gold nanoparticles on PECVD tyrosine film; inset shows gold nanoparticles within $2 \times 2\,\mu m^2$ typical scan used for spot EDX measurements.

2.4. Micropatterning of Tyrosine Coatings

Patterning of the tyrosine during plasma deposition was done by securing a 1000-mesh TEM grid with $10 \times 10\,\mu m^2$ square openings to the substrate to act as a mask during the PECVD deposition of L-tyrosine. This method allowed regular patterns to be created on the silicon surface across the entire masked region (Figure 7a and b). AFM section analysis of the patterned area shows that the peak height of the square tyrosine regions was 80 nm (Figure 7c). The four missing squares were caused by defects in the grid that prevented polymer deposition. This selective deposition demonstrates the ability to introduce, control, and reproduce changes to the patterned system with the mask during deposition (Figure 7C).

After exposure of the patterned tyrosine substrate to the gold chloride solution, it was seen that these patterns are capable of selectively reducing gold nanoparticles on the tyrosine-coated regions, while leaving the areas of exposed silicon relatively clean and free of nanoparticles, which creates density controlled regular regions of gold nanoparticles selectively reduced on the squared surface areas (Figure 8a and b). The nanoparticles observed in these regions were 2–3-nm-sized nanoparticles covering the surface and match the results seen on the uniform tyrosine films, with larger gold aggregates also present (Figure 8c).

However, the small feature sizes of the patterning results in some delamination of the tyrosine film during removal of the mask and exposure to the gold chloride solution. This delamination primarily occurred at the edges of the squares and was evidenced by the non-uniformity of the coating between the squares. As the TEM grid was secured only around the edges of the substrate, there was some tyrosine that permeated under the masked area which left a thin residual film in the valleys between the raised areas with a thickness of less than 10 nm. These are weaker regions that are prone to delamination.

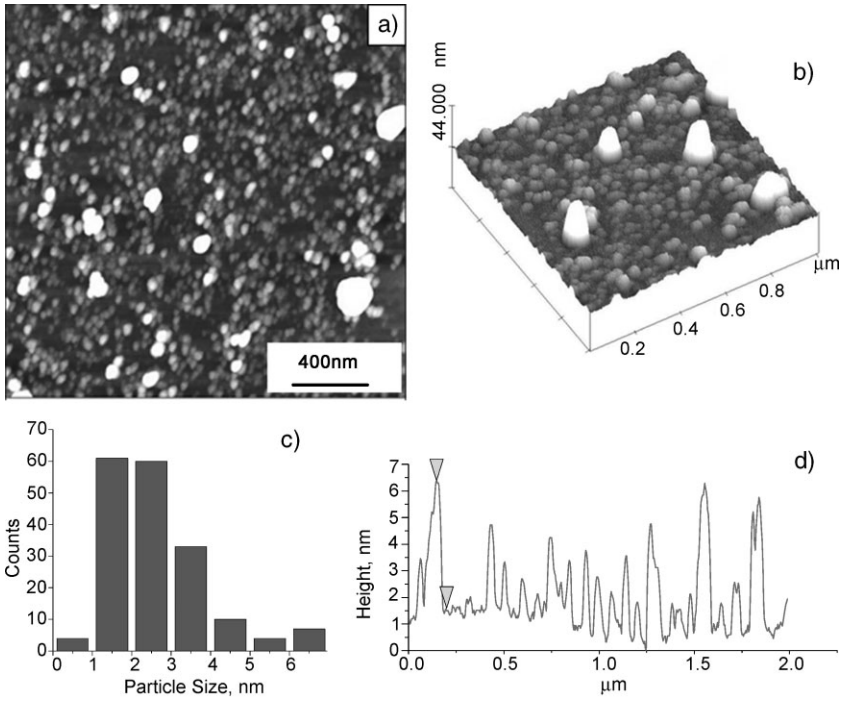

Figure 5. Analysis of gold nanoparticles after reduction on PECVD tyrosine film. AFM images a) $2 \times 2\,\mu m^2$, $Z = 15$ nm and b) 3D $1 \times 1\,\mu m^2$, $Z = 15$ nm. c) Histogram of particle size distribution on tyrosine surface. d) Sample of cross-section analysis from AFM image showing measured height of the nanoparticles.

2.5. Alternative Substrates for PECVD Tyrosine Coatings

By using PECVD to deposit tyrosine, we were able to create functional coatings not only on atomically flat silicon wafers

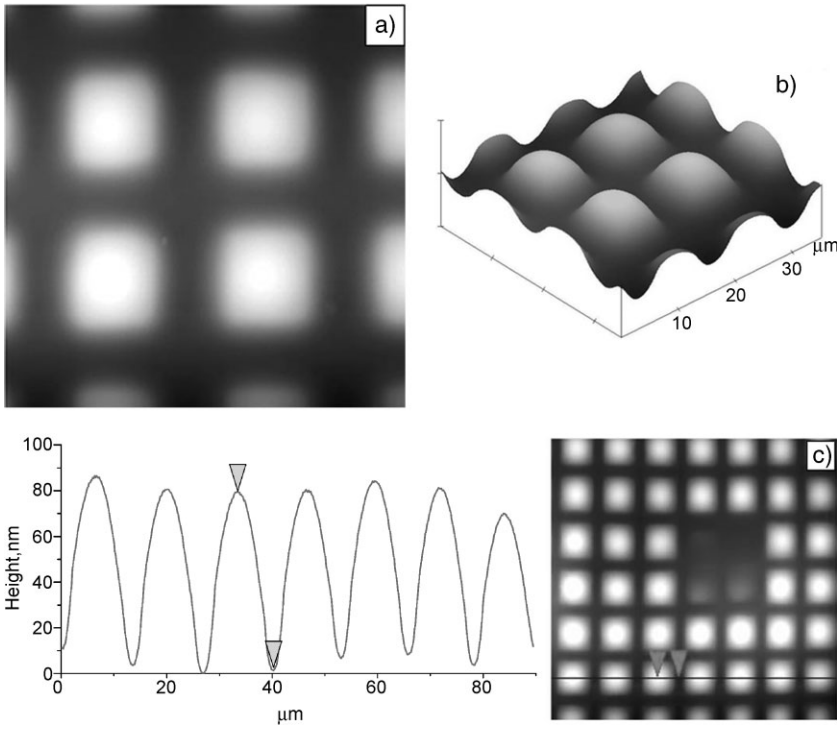

Figure 7. Micropatterned tyrosine films: a) patterned tyrosine $35 \times 35\ \mu m^2$ scan $Z = 230$ nm. b) 3D scan of patterned area shown in a). c) Cross-section analysis of patterned area showing heights of regions.

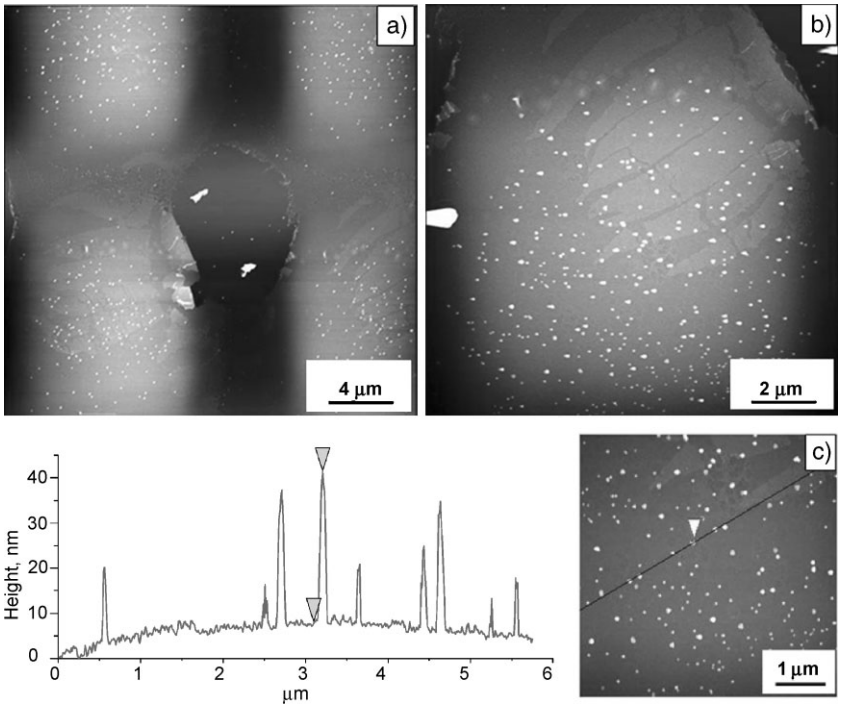

Figure 8. AFM images of gold nanoparticles grown on micropatterned film: a) $Z = 60$ nm, b) $Z = 90$ nm, c) $Z = 60$ nm. Height of gold nanoparticles measured is 33 nm.

but also on specimens of commercial PTFE and nitrocellulose (discussed here) along with PDMS, polystyrene, glass, woven silk, and polyethylene. The specimens coated represent a wide range of conventional plastics. The results for these materials were favorable and warrant further study into their specific coating and reduction potential, which would be valuable. Through further study, we hope to determine where the limits of this coating technique lie. However, we have already observed that PECVD is a faster coating method and offers more complete coverage than solution treatment with polytyrosine, as seen in comparative experiments.

While all samples tested supported stable plasma coatings and gold reduction, PTFE and nitrocellulose are characterized here for preliminary studies as they proved to be promising and provided the clearest optical images of the coating and reduction process which we highlighted visually, since both show differences in the surface appearance (Figure 9). By showing the ability to make robust plasma-polymerized tyrosine coatings and gold nanoparticles on different surfaces, there is a demonstrated potential for the reduction of metal nanoparticles on materials that had not previously been able to support this process without some type of surface modification. Four samples were prepared for the optical demonstration: the bare substrate, the bare substrate exposed to a solution of gold chloride, tyrosine deposited on the substrate, and the tyrosine-coated substrate exposed to gold chloride. The reduction of gold nanoparticles on the surface by the tyrosine is evidenced by the color change between the samples of tyrosine-coated and tyrosine-uncoated nitrocellulose exposed to gold chloride. A drastic change in color is seen in the tyrosine-coated surface, where a deep red color is clear, in contrast to almost no color change on the uncoated sample (Figure 9). Differences are also evident on the samples that have not been exposed to gold chloride. Both the tyrosine-coated nitrocellulose and PTFE were seen to be light yellow, whereas the uncoated samples were bright white. This is a striking example of the effectiveness of plasma-deposited tyrosine at reducing gold nanoparticle across an entire surface.

To confirm the presence of the tyrosine film and gold nanoparticles on the PTFE,

NANO MICRO small

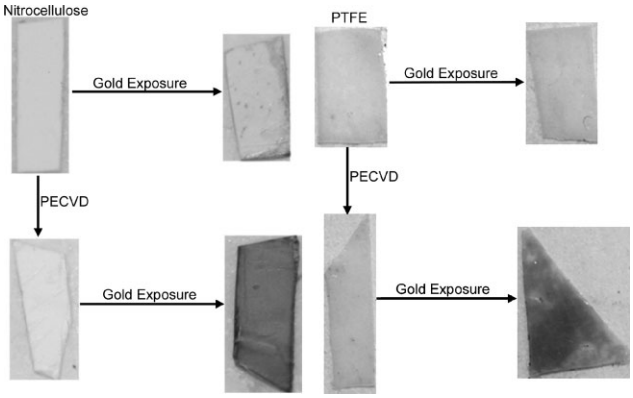

Figure 9. Optical images of nitrocellulose (left) and PTFE (right) coated with tyrosine coating and exposed to gold chloride. The unmodified substrate is first exposed to the gold solution with no tyrosine coating. A PECVD coating of tyrosine is placed on the blank substrate and exposed to gold chloride. This visibly highlights the reduction of gold nanoparticles on the surface by the tyrosine.

nitrocellulose, and silicon substrates, XPS analysis was conducted to identify key components of the material. Examples of spectra obtained from the tyrosine coating with reduced gold nanoparticles on silicon and PTFE clearly show distinct peaks for gold and nitrogen (Figure 10a and b, Table 1). The essential marker from the tyrosine is the nitrogen indication from the N 1s peak, which is derived from the amine group of the tyrosine. Au 4f and Au 4d peaks are seen on the samples only after tyrosine has been deposited and the sample exposed to gold chloride. The blank substrates exposed to gold chloride show no gold, except in the case of nitrocellulose, which is capable of a small amount of reduction on its own (Table 1). However, gold reduction is much more pronounced after the addition of the tyrosine. The control samples of the other blank substrates exposed to gold chloride do not show the presence of gold which indicates that reduction of gold nanoparticles is a direct result of the tyrosine present on the surface and not only of the substrate functionality. The small amount of chlorine detected was a result of exposure to the gold chloride solution.

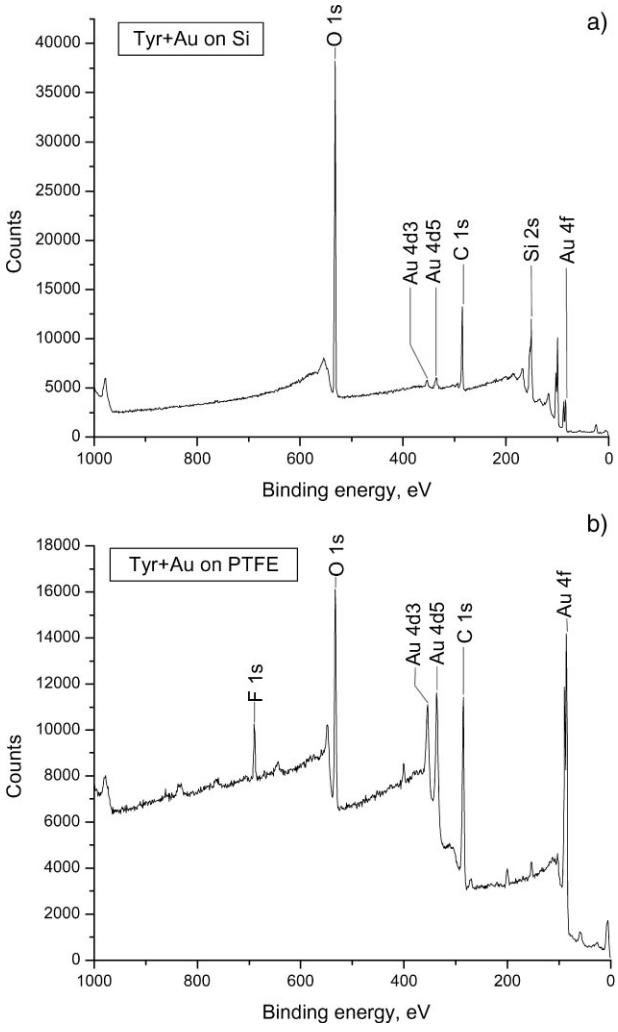

Figure 10. a) XPS of PECVD tyrosine after the reduction of gold on silicon. b) XPS of PECVD tyrosine after the reduction of gold on PTFE.

Table 1. Atomic percentages showing composition of films on PTFE, nitrocellulose, and silicon by XPS.[a]

	Si 2p	Si 2s	C 1s	O 1s	N 1s	Au 4f	Au 4d5	Au 4d3	Au 5p3	F 1s	Cl 2p
PTFE	–	–	42.61	4.24	–	–	–	–	–	53	–
PTFE + Au	–	0.29	32.33	2.77	–	0.1	–	–	–	63.59	–
PTFE + Tyr	4.73	4.27	47.12	16.53	4.12	–	–	–	–	–	–
PTFE + Tyr + Au	–	3.65	38.38	29.37	2.7	4.44	3.56	5.34	3.68	3.45	1.6
Si	–	36.71	17.72	32.5	–	–	–	–	–	–	–
Si + Au	–	31.66	17.53	30.72	–	–	–	–	–	–	–
Si + Tyr	–	5.4	70.82	19.73	3.44	–	–	–	–	–	–
Si + Tyr + Au	–	28.73	21.51	27.45	–	0.53	0.44	0.54	–	–	–
Nitrocellulose	–	–	53.03	38.84	7.33	–	–	–	–	–	–
NC + Au	–	–	46.59	40.59	8.53	0.59	0.44	1.28	–	53	–
NC + Tyr	0.89	0.71	52.18	16.98	5.59	–	–	–	–	–	–
NC + Tyr + Au	–	–	53.74	24.01	6.43	1.99	1.96	2.35	–	–	3.01

[a] The spectra of the uncoated substrate, the uncoated substrate exposed to gold chloride solution (+Au), the substrate coated with tyrosine via PECVD (+Tyr), and the tyrosine-coated substrate after exposure to gold chloride solution (+Tyr + Au).

This analysis demonstrates the effectiveness of PECVD for tyrosine deposition and shows that the resulting film has good adhesion to many substrates, enabling the reduction of gold nanoparticles on these surfaces. This type of coating-reduction system allows simple surface modification and has many potential applications in tunable optical coatings and chemical detection. Moreover, we suggest that tyrosine plasma coatings can potentially be applied for gold reduction to many other substrates as well, offering a wide range of surfaces suitable for applications involving plasma coating and reduction of gold nanoparticles.

3. Conclusions

This study shows that PECVD provides a facile method for the deposition of tyrosine monomer for biometallization. Smooth, conformal, and uniform films were created quickly and reliably with this method. Additionally, PECVD is a one-step coating process that completely eliminates the need for any wet chemistry in the fabrication of tyrosine films, as the solid monomer can be heated and sublimed directly into the plasma stream during deposition. The plasma deposition method described results in a highly crosslinked tyrosine coating on the substrates. This interlocking of the molecules contributes significantly to the stability and robustness of the films.

The plasma-deposited tyrosine films show excellent robustness when exposed to gold chloride for biometallization, demonstrating the versatility and durability of this surface-coating technique for biometallization on a variety of substrates from silicon to PTFE. Patterning of the tyrosine films demonstrates that the PECVD-mask system combination is an effective method for creating patterned regions on the substrate that are capable of selectively reducing gold nanoparticles on the surface. These results demonstrate the potential for precisely directing the areas of growth of gold nanoparticles that is controlled simply by the mask. While only square patterns were created and studied herein, there is a much larger range of potential shapes and patterns that can be created, and this method could possibly be extended to such complex shapes as seen in micro- and nanoscale photolithography patterning.

This type of inorganic reduction can be extended from gold nanoparticles to other minerals and metals by using different amino acids and peptides to make PECVD films. We suggest that robust PECVD films can potentially be made from a number of different monomers and even short peptides, each selected for a specific function and binding ability. Mixtures of amino acid monomers or selective patterning during deposition can potentially be used to deposit several different types of inorganic material on or in close proximity to one another, allowing different metal nanoparticles and bimetallic materials to be precisely placed to tune optical or conductive properties. Plasma-polymerized polyamino acid coatings have a great potential for tunable organic/inorganic composite material fabrication, as the inorganic-substrate-reducing amino acid monomer can be conformally coated onto any substrate. Functionalized PECVD films that allow biometallization may see applications in tunable optical device layers, wavelength-specific filters, selective surfaces for optical and sensing applications such as stacked layers that act as broad-spectrum filters for electromagnetic radiation.

4. Experimental Section

Materials: L-Tyrosine was purchased from Sigma–Aldrich and used as received in all processes described (Figure 2). Depositions were done on highly polished single-crystal {100} silicon substrates (University Wafer) cleaned in piranha solution (caution! 3:1 conc. H_2SO_4 and 30% H_2O_2). Additional substrates used for deposition were cut from stock sheets of polytetrafluroethylene (PTFE), polyethylene, polydimethylsiloxane (PDMS), polystyrene, woven silk fibers, glass, and nitrocellulose.

The PECVD vacuum chamber was set up for plasma-enhanced coatings by sublimation according to an established procedure.[48,57,58] The chamber was custom built and used a capacitively coupled radio-frequency power source at 13.56 MHz to generate the plasma between two aluminum electrodes. The L-tyrosine monomer was placed in a tantalum heating boat in the PECVD chamber. Power was applied to the heating boat to heat the monomer through electrical resistance up to a temperature of 300 °C, subliming the monomer for induction into the plasma. For best tyrosine film results discussed herein, the chamber plasma was run at 60 W with an argon flow rate of 10 cm^3 min^{-1} (99.99% purity) at a pressure of 2.0 Pa for all tyrosine sublimation depositions. Patterning of the tyrosine was done by securing a 1000 mesh copper TEM grid to the silicon wafer. The deposition was carried out according to the listed procedure, and the grid was removed upon completion.

Gold chloride ($HAuCl_4$) (30% Aldrich) was diluted in borate buffer (pH 10) to a concentration of 0.1 M. This solution was then placed onto the PECVD-coated tyrosine film and allowed to absorb for a specified length of time between 1 and 5 days. After deposition, the sample was rinsed with nanopure water (18 MΩ cm^{-1}) and dried under nitrogen.

Characterization: FTIR measurements were done on a Perkin-Elmer Spectrum 2000 FT-IR spectrometer in transmission mode. Samples were prepared on double-sided polished silicon wafers to minimize the background signal. The wavenumber range was from 500 to 5000 cm^{-1}, and 1000 scans were averaged for each plot. A Phillips XL series SEM equipped with an EDAX detector was used for determining the composition of the nanoparticles. AFM images were collected by using a Dimension 3000 microscope with a Nanoscope IIIa controller according to an established procedure.[59,60] A light tapping regime was used in air on all samples to avoid surface damage. Triangle silicon cantilevers (MikroMasch) with a nominal spring constant of 50 N m^{-1} were used for all measurements.

Thickness measurements were carried out with a Woollam M2000U multiangle spectroscopic ellipsometer for angles 65, 70, and 75°. Optical constants n and k were determined by using the Cauchy model for wavelengths from 200 to 1000 nm. XPS was performed on an M-Probe Surface Science XPS spectrometer

NANO MICRO small

using charge neutralization. Spectra were collected from 0 to 1000 eV at 1-eV steps at a spot size of 800 μm and averaged over 15 scans.

Acknowledgements

This work was supported by the Air Force Office for Scientific Research, Air Force Research Laboratory, and the AFRL Bio-X STT program. The authors thank Eugenia Kharlampieva for technical assistance with FTIR and related discussions and Hao Jiang for technical assistance with plasma depositions and spectra analysis. The authors also thank Srikanth Singamaneni and Ray Gunawidjaja for useful discussions.

[1] R. Naik, S. J. Stringer, G. Agarwal, S. E. Jones, M. O. Stone, *Nat. Mater.* **2002**, *1*, 169.
[2] J. M. Slocik, R. R. Naik, *Adv. Mater.* **2006**, *18*, 1988.
[3] J. M. Slocik, R. R. Naik, M. O. Stone, D. W. Wright, *J. Mater. Chem.* **2005**, *15*, 749.
[4] N. Loges, G. Karlheinz, L. Nasdala, W. Tremel, *Langmuir* **2006**, *22*, 3073.
[5] A. L. Boskey, *Connect. Tissue Res.* **2003**, *44*, 5.
[6] H. P. Jennissen, M. Laub, *Mater. Wiss. Werkst.* **2007**, *38*, 1035.
[7] Y. Jiang, D. Yang, L. Zhang, L. Li, Q. Sun, Y. Zhang, J. Li, Z. Jiang, *Dalton Trans.* **2008**, 4165.
[8] H. H. Klump, K. Koch, C. T. Lin, *S. Afr. J. Sci.* **2006**, *102*, 264.
[9] T. Ueno, N. Yokoi, S. Abe, Y. Watanabe, *J. Inorg. Biochem.* **2007**, *101*, 1667.
[10] M. B. Dickerson, K. H. Sandhage, R. R. Naik, *Chem. Rev.* **2008**, *108*, 4935.
[11] a) L. Addadi, S. Weiner, *Angew. Chem.* **1992**, *104*, 159; b) L. Addadi, S. Weiner, *Angew. Chem.* **1992**, *104*, 159; *Angew. Chem. Int. Ed. Engl.* **1992**, *31*, 153.
[12] T. Prozorov, S. K. Mallapragada, B. Narasimhan, L. Wang, P. Palo, M. Nilsen-Hamilton, T. J. Williams, D. A. Bazylinski, R. Prozorov, P. C. Canfield, *Adv. Funct. Mater.* **2007**, *17*, 951.
[13] S. Areva, T. Peltola, E. Säilynoja, K. Laajalehto, M. Lindén, J. B. Rosenholm, *Chem. Mater.* **2002**, *14*, 1614.
[14] J. Ekeroth, A. Borgh, P. Konradsson, B. J. Liedberg, *J. Colloid Interf. Sci.* **2002**, *254*, 322.
[15] X. Mo, M. P. Krebs, S. M. Yu, *Small* **2006**, *4*, 526.
[16] G. Hodes, *Adv. Mater.* **2007**, *19*, 639.
[17] J. M. Slocik, M. O. Stone, R. R. Naik, *Small* **2005**, *11*, 1048.
[18] H. Lee, S. M. Dellatore, W. M. Miller, P. B. Messersmith, *Science* **2007**, *318*, 426.
[19] N. Wangoo, K. K. Bhasi, S. K. Mehta, C. R. Suri, *J. Colloid Interf. Sci.* **2008**, *323*, 247.
[20] E. Kharlampieva, J. M. Slocik, T. Tsukruk, R. R. Naik, V. V. Tsukruk, *Chem. Mater.* **2008**, *20*, 5822.
[21] K. Ariga, J. P. Hill, M. V. Lee, A. Vinu, R. Charvet, S. Acharya, *Sci. Technol. Adv. Mater.* **2008**, *9*, 014109.
[22] V. V. Tsukruk, *Prog. Polym. Sci.* **1997**, *22*, 247.
[23] G. Decher, *Science* **1997**, *277*, 1232.
[24] C. Jiang, V. V. Tsukruk, *Adv. Mater.* **2006**, *18*, 829.
[25] *Multilayer Thin Films: Sequential Assembly of Nanocomposite Materials*, Eds.: G. Decher, J.-M. Lehn, J. Schlenoff, Wiley-VCH, Weinheim **2003**.
[26] F. Hua, Y. Lvov, T. Cui, *Thin Solid Films* **2004**, *449*, 222.
[27] D. Lee, M. F. Rubner, R. E. Cohen, *Nano Lett.* **2006**, *6*, 2305.
[28] B. M. Rybak, K. N. Bergman, M. Ornatska, K. L. Genson, V. V. Tsukruk, *Langmuir* **2006**, *22*, 1027.
[29] E. Kharlampieva, T. Tsukruk, J. M. Slocik, H. Ko, N. Poulsen, R. R. Naik, N. Kröger, V. V. Tsukruk, *Adv. Mater.* **2008**, *20*, 3274.
[30] E. Kharlampieva, J. M. Slocik, S. Singamaneni, N. Poulsen, N. Kroger, R. R. Naik, V. V. Tsukruk, *Adv. Funct. Mater.* in press.
[31] T. Fukuoka, Y. Tachibana, H. Tonami, H. Uyama, S. Kobayashi, *Biomacromolecules* **2002**, *3*, 768.
[32] E. Katchalski, M. J. Sela, *J. Am. Chem. Soc.* **1953**, *75*, 5284.
[33] M. Seyama, Y. Iwasaki, S. Ogawa, I. Sugimoto, A. Tate, O. Niwa, *Anal. Chem.* **2005**, *77*, 4228.
[34] D. Klee, Z. Ademovic, A. Bosserhoff, H. Hoecker, G. Maziolid, H.-J. Erli, *Biomaterials* **2003**, *24*, 3663.
[35] S. Tone, T. Masawaki, T. Hamada, *J. Memb. Sci.* **1995**, *103*, 57.
[36] B. M. Wickson, J. L. Brash, *Colloids Surf.* **1999**, *156*, 201.
[37] S. Kurosawa, E. Tawar-Kondo, N. Minoura, N. Kamo, *Sens. Actuators, B: Chem.* **1997**, *43*, 175.
[38] S. Tone, T. Masawaki, K. Eguchi, *J. Membrane Sci.* **1996**, *118*, 31.
[39] J. M. Slocik, E. R. Beckel, H. Jiang, J. O. Enlow, J. S. Zabinski, T. J. Bunning, R. R. Naik, *Adv. Mater.* **2006**, *18*, 2095.
[40] S. J. Oldenberg, S. L. Westcott, R. D. Averitt, N. J. Halas, *J. Chem. Phys.* **1999**, *111*, 4729.
[41] J. Cho, F. Caruso, *Chem. Mater.* **2005**, *17*, 4547.
[42] H.-H. Yu, J. W. Hutchinson, *Thin Solid Films* **2003**, *423*, 54.
[43] Y. Eom, L. Boogh, V. Michaud, P. Sunderland, J.-A. Månson, *Polym. Eng. Sci.* **2000**, *40*, 1281.
[44] H. Yasuda, *Plasma Polymerization*, Academic Press, Inc. New York 1985.
[45] T. Williams, M. W. Hayes, *Nature* **1966**, *209*, 769.
[46] Y. Zubavichus, A. Shaporenko, M. Grunze, M. Zharnikov, *J. Phys. Chem. B* **2007**, *111*, 9803.
[47] S. Singamaneni, M. C. LeMieux, H. P. Lang, C. Gerber, Y. Lam, S. Zauscher, P. G. Datskos, N. V. Lavrik, H. Jiang, R. R. Naik, T. J. Bunning, V. V. Tsukruk, *Adv. Mater.* **2008**, *20*, 653.
[48] M. C. LeMieux, M. E. McConney, Y.-H. Lin, S. Singamaneni, H. Jiang, T. J. Bunning, V. V. Tsukruk, *Nano Lett.* **2006**, *6*, 730.
[49] H. Jiang, W. E. Johnson, J. T. Grant, K. Eyink, E. M. Johnson, D. W. Tomlin, T. J. Bunning, *Chem. Mater.* **2003**, *15*, 340.
[50] S. Kurosawa, N. Kamo, D. Matsui, Y. Kobatake, *Anal. Chem.* **1990**, *62*, 353.
[51] J. A. Theil, J. G. Brace, R. W. Knoll, *J. Vac. Sci. Technol. A* **1994**, *12*, 1365.
[52] J. D. S. Newman, G. J. Blanchard, *J. Nanopart. Res.* **2007**, *9*, 861.
[53] K.-K. Chia, R. E. Cohen, M. F. Rubner, *Chem. Mater.* **2008**, *20*, 6756.
[54] M. A. Hernandez-Perez, C. Garapon, C. Champeaux, J. C. Orlianges, *J. Phys: Conf. Ser.* **2007**, *59*, 724.
[55] L. I. Grace, R. Cohen, T. M. Dunn, D. M. Lubman, M. S. de Vries, *J. Mol. Spectrosc.* **2002**, *215*, 204.
[56] a) P. Crews, J. Rodríguez, M. Jaspars, *Organic Structure Analysis*, Oxford University Press, New York 1998, p. 354; b) E. Pretsch, P. Bühlmann, C. Affolter, *Structure Determination of Organic Compounds*, Springer, Berlin **2000**, p. 395.
[57] J. O. Enlow, H. Jiang, J. T. Grant, K. Eyink, W. Su, T. J. Bunning, *Polymer* **2008**, *49*, 4042.
[58] P. Haaland, J. Targove, *Appl. Phys. Lett.* **1992**, *61*, 34.
[59] V. V. Tsukruk, *Rubber Chem. Technol.* **1997**, *70*, 430.
[60] V. V. Tsukruk, D. H. Reneker, *Polymer* **1995**, *36*, 1791.

Received: December 10, 2008
Revised: December 30, 2008
Published online: March 6, 2009

